Elucidating the Interaction of CO_2 in the Giant Metal-Organic Framework MIL-100 through Large-Scale Periodic *Ab Initio* Modelling

Maddalena D'Amore[a], Bartolomeo Civalleri[a]*, Ian J. Bush[b], Elisa Albanese[a]†, Matteo Ferrabone [a]¥

[a] Dipartimento di Chimica e Centro Interdipartimentale NIS, Università di Torino, Via P. Giuria 7, 10125 Torino
[b] Oxford e-Research Centre, Department of Engineering Science, University of Oxford, 7 Keble Road, Oxford, OX1 3QG

ABSTRACT: In this work, we have tackled the challenging task of the *ab initio* modelling of a gigantic metal-organic framework (MOF). The structural features of MIL-100(M^{III}) with different metals (i.e. M^{III}=Al, Sc, Cr, Fe) and the interaction of CO_2 with the unsaturated coordination metal sites were investigated by means of large scale quantum mechanical calculations with hybrid HF/DFT methods augmented with an atom-atom pairwise dispersion correction in a fully periodic approach. In doing this, we took advantage of the high scalability of the massively parallel version of the CRYSTAL code. Overall results are in good agreement with experiment, in particular for the predicted structures, while some discrepancies have been found for adsorption energies in the case of MIL-100(Cr) and MIL-100(Sc). We argue that this is due to a deviation of the ideal model structure of MIL-100 adopted in this work from the actual synthesized material. This is also supported by additional calculations on a MOF with similar adsorption sites and computed data from literature. Above all, we demonstrate that *ab initio* modelling of the structure and properties of MOFs can now be performed on very large and complex frameworks.

Introduction

Some decades ago Metal Organic Frameworks (MOFs) emerged as a new technologically interesting family of materials that belong to the broad class of coordination polymers. Since then, their structure, properties and use in next-technology applications have been widely discussed in review articles and many special issues (see Ref. [1,2,3,4] and citations therein). MOFs are built of inorganic moieties, usually a metal or a cluster, and organic, polytopic ligands, acting both as secondary building units that are linked throughout space to form a tridimensional framework [5]. In many cases they possess a stable and porous crystalline structure that can show a high or even ultra-high degree of porosity [6]. One of the major advantages of MOFs is the chemical versatility of the combination of inorganic and organic components that imparts the material an extraordinary structural variety. The search for MOFs with specific structure-property relationships has led to the syntheses of a huge number of new MOFs with different sizes from small to medium and even giant MOFs [7]. They have then been tailored to display such peculiar features (e.g. porosity and ordered structure) optimally [8]. It is not surprising that a hot topic area in which MOFs have played a major role in the last years is gas capture and storage and gas mixtures separation [9]; in particular, they show larger CO_2 adsorption capacity at high pressures than most zeolites and carbon materials due to their higher surface area and pore volume[10,11,12].

From a modelling viewpoint, computational methods can be employed to estimate the adsorption capacity of these nano-porous materials and accurately predict selectivity and uptake of gases on the basis of atomistic level knowledge of their structure and properties[13,14,15]. As in some cases this might be out of reach of experimental methods, it may represent a basis upon which to design specifically tailored frameworks. With this in mind, simulations have been already used to characterize MOFs for gas adsorption together with its mechanisms [16,17], with the methods employed ranging from molecular mechanics (MM) with both classical and semi-classical force-fields[18,19,20], to quantum mechanical (QM) methods, passing through QM/MM approaches.

Molecular mechanics methodologies have the advantage of being very cost effective for MOFs. For instance, by using *ad hoc* modified versions [21,22] of well-behaved force fields, there are many theoretical studies of CO_2 adsorption in MOFs using Grand Canonical Monte Carlo (GCMC) simulations reported in the literature [23,16]. These are based on atomistic potential parameters and a partial charge model.

Since many MOFs have very large and complex structures and quantum mechanical calculations on these structures can become very demanding, QM/MM approaches have been also proposed in order to investigate the interaction of molecules with the unsaturated metal centres. These methods have been used for studies of adsorption and especially catalysis [24,25–29]. A small region around the active site is treated by the expensive but accurate QM methods, while the rest of the system is treated by MM force fields, which may represent a cheaper solution. The problem is then to develop methods to handle the boundary between the two methods, but significant progress has been made here [29].

However, in spite of the cost, quantum mechanical modelling of the adsorption in MOFs has been successfully employed in the recent years by means of a periodic approach [30,31,32,33,34,35,36,37,38,39,40], which is the natural choice for crystalline systems as MOFs. Nevertheless such work has previously been limited to small to medium size frameworks and their interaction

with small molecules. Alternatively, cluster models have also been adopted (see for instance ref. [41], which is relevant for the present work, *vide infra*). Although in this case higher-level QM methods than DFT approximations can be used, the size of both the cluster and adsorbed molecule can pose a limit in modelling adsorption in MOFs, in particular when the adsorbate can interact with the framework. In addition, when cutting the cluster dangling bonds must be properly saturated.

Therefore, here we report a step forward in the *ab initio* modelling of MOFs by investigating the adsorptive capacity of the so-called *giant* MOFs through a fully periodic quantum mechanical approach. Among the giant MOFs, MIL-100 and MIL-101[42] are amongst the most representative. They are comprised of oxo-centered trinuclear units (hereafter denoted as trimeric units, TU) of trivalent metals M^{III} octahedral connected with 1,3,5-BTC (benzene-1,3,5-tricarboxylic acid also known as trimesic acid) and 1,4-BDC (benzene-1,4-dicarboxylic acid), respectively. They were originally synthesized with Cr as the metal ion, but then other isoreticular frameworks were obtained with different metals (i.e. M^{III}=Al,[43] Sc,[44,45,46] V,[47] Mn,[48] Fe,[49,50]), in particular for MIL-100.

In this study, we focused on MIL-100 whose crystallographic and secondary building units are shown in Figure 1. It is a highly porous material with cages of different size from micro- (6.5 Å) to meso-pores (25.0-30.0 Å) and featuring a surface area of 3340 m^2/g, that is 3 times larger than the values measured for the MCM-41 inorganic mesoporous materials[42] For this reason such a *giant* MOF is also denoted as *mesoporous* MOF. Furthermore, it has a very large unit cell that contains around 2800 atoms in the primitive cell (see Figure 1) which makes it a very challenging system to be modelled by means of quantum mechanical methods. In addition, as we mentioned above, one of the hottest topics in MOFs research is their application in clean energy and environmental protection, as for CO_2 capture and sequestration. An important aspect in maximizing the uptake of gases within porous MOF crystals is to increase the number of adsorption sites. Due to its *giant* framework, MIL-100 is characterized by the presence of more than 100 coordinatively unsaturated (CUS) metal atoms that are exposed at the inner surface of the pores in the unit cell. Notably, MIL-100(Cr) also shows the highest adsorption enthalpy among a large set of MOFs [11].

From a computational viewpoint, there are at least two specific challenges related to the present work: the importance of accurately predict the interaction between the adsorption site and carbon dioxide by including dispersive forces and, above all, the hard task of tackling the large system size of MIL-100.

To cope with the former aspect, an accurate, reliable yet simple, cheap and widely used method to include dispersion interactions was adopted. It consists of augmenting the semilocal or hybrid functional with an atom-pairwise term of the form $f(r^{-6})$ as in the semi-empirical DFT-D family of methods of Grimme et al. [51,52,53] that have been extensively applied to both molecular complexes[51,54,55] and extended systems [56,57] where the London dispersion interactions play a major role [58,59]. It is also worth mentioning that dispersion corrected DFT-D methods have been successfully applied to model the adsorption of CO_2 in several MOFs [60,61,33,62,63,64,65]. Remarkably, the DFT-D approach has been shown to give results in good agreement with CCSD(T) calculations [66].

The second challenge is the most demanding one; indeed the system size requires an efficient and highly parallelized code in order to make calculations feasible. To this end, we have adopted the CRYSTAL periodic code [67] in its massively parallel version (MPP), specifically tailored to achieve an excellent scalability on HPC systems [68]. It can treat very large unit cell systems with large memory requirements, as the matrices in the reciprocal space are fully distributed over the processes and parallel Linear Algebra Library routines (ScaLapack) are used for diagonalization, matrix products, Choleski decomposition and other operations. The required memory per process has also been strongly reduced for large systems containing thousands of atoms per cell. In addition, CRYSTAL adopts atom-centered Gaussian functions and this constitutes a clear advantage compared to a plane-waves based approach for very large highly porous systems. Furthermore, the code allows for an accurate and efficient evaluation of the exact Hartree Fock exchange needed for hybrid HF/DFT methods as with the B3LYP[69], PBE0[70] or M06 [71] functionals, to mention a few.

Hence, the purpose of this work is twofold. Firstly, we predict the structural features of MIL-100(M^{III}) with different metals (i.e. M^{III}=Al, Sc, Cr, Fe) and then analyse the specific interaction of CO_2 with the unsaturated coordination metal sites by means of quantum mechanical calculations with hybrid HF/DFT methods augmented with an atom-atom pairwise dispersion correction. Secondly, we show that such calculations are currently affordable and can be performed even on gigantic MOFs as MIL-100. Overall, we demonstrate that modelling the structure and properties of MOFs with very large and complex frameworks is now possible and affordable.

Models and Methods

Models

MIL-100 has the formula $M^{III}_3X\,(H_2O)_2\,O\,[C_6H_3(CO_2)_3]_2{\cdot}n\,H_2O$ (M^{III}=Al, Sc, V, Mn, Cr, Fe) and it was first synthesized by G. Ferey and co-workers [42] with Cr as the metal and F^- as counterions to neutralize the positively charged inorganic units. Later, isomorphous structures of MIL-100 were prepared with different metal atoms, namely: Al, Sc, V, Mn, Fe, with either F^- or OH^- as the counterion [43,45,46,48,49].

MIL-100 is built by a combination of an inorganic trimeric unit (TU) formed by a trivalent metal and a μ^3-Oxygen, and trimesate organic unit acting as linker (Figure 1). These two secondary building units (SBU) assemble to form a bigger SBU denoted "supertetrahedron" that creates a complex tridimensional porous structure. The resulting framework has the topology of the MTN zeolite [42] with two sets of "mesoporous" cages, namely: a small one with a diameter of 25 Å and a large one with a diameter of 29 Å. Cages are connected with pentagonal and hexagonal windows [42].

From XRPD measurements,[42] it is known that MIL-100(M^{III}) crystallizes in a cubic lattice with *Fd-3m* space group. Actually, the cubic symmetry as observed from experiments is due to a structural disorder of the counterion and coordination waters. To build a 'realistic' model of MIL-100(M^{III}) we removed all water molecules and then counterions were positioned on one of the metal of each trimeric unit. For sake of simplicity, we decided to model MIL-100(M^{III}) with fluoride as the counterion and keep the number of symmetry operators as large as possible to mitigate the computational burden. In doing this, the positioning of the counterions led to a symmetry lowering that results in the tetragonal symmetry subgroup *I41/amd* (Space group 141) which

still retains sixteen symmetry operators. In the resulting structure, all fluorine atoms are located in the hexagonal windows of the framework (vide infra).

Our final model structure of MIL-100(M^{III})-F is then tetragonal with 16 residual symmetry operators. The asymmetric unit contains 16 metal atoms that are not equivalent by symmetry. Among them, seven metal atoms are linked to the counterion (i.e. F^-) while the remaining are coordinatively unsaturated sites. It follows that in the unit cell there are 68 trimeric units with 204 metal atoms, but only 136 are available to interact with probe molecules such as CO_2: they constitute the adsorption sites and act as Lewis acid centres. In total, the primitive unit cell contains 2788 atoms.

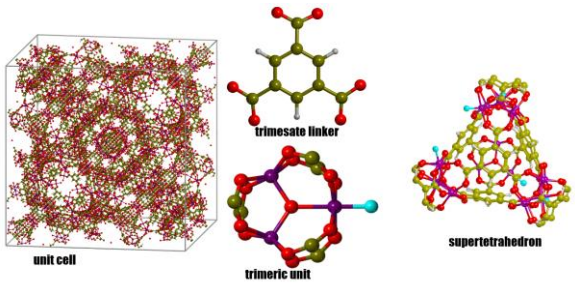

Figure 1 MIL-100(M) crystallographic unit cell, on the left, along with the inorganic and organic building blocks, in the middle, and the actual secondary building unit of the framework known as "supertetrahedron" [45]. H, C, O, F and M, are in white, light brown, red, light blue and violet, respectively.

As anticipated in the Introduction, four different metal species M^{III} (M^{III}=Al, Sc, Cr, Fe) have been investigated in MIL-100 periodic models. Special attention has been devoted to model the structure of MIL-100 for spin polarized transition metals as Cr and Fe because of the possibility to have unit cells with various magnetic orderings. The electronic structure of the different unit cells were modelled by taking into account some experimental evidence about magnetic couplings within the TU in MIL-100(Fe)-F. For sake of brevity, more details are given as Supplementary Information (ESI).

Computational details

All calculations were carried out by using the distributed-data massively parallel version of CRYSTAL software (MPPCRYSTAL) [67,68,72,73], we adopted hybrid HF/DFT theoretical methods. The B3LYP functional augmented with an empirical correction to include dispersion interactions (i.e. +D*) [56] was adopted in combination with a triple-zeta quality pob-TZVP/6-311G(d,p) basis set, namely: a 6-311G** Pople basis set for the organic part of the framework (i.e. H, C and O) and the Peintinger-Oliveira-Bredow basis set [74] on the metal atom. For the CO_2 molecule, a TZP basis set was employed [75]. The overall basis set contains more than 50000 basis functions (BFs). The numerical accuracy for integral calculations and SCF convergence was set high enough to guarantee and accurate determination of the electronic structure. This is crucial for spin polarized systems (i.e. MIL-100(Cr) and MIL-100(Fe) in that magnetic solutions involve very low differences in energy ΔE of the order of 10^{-4} Hartree.

The model structure of MIL-100(M^{III}) as described in the previous section was fully optimized (i.e. lattice parameters and atomic positions) both "as it is" and with 8 and 16 CO_2 molecules in the unit cell (vide infra), keeping the residual symmetry of the system. The adsorption energy was evaluated through a supramolecular approach. Basis set superposition error was taken into account through the Boys-Bernardi counterpoise correction [76]. Single point energy calculations on the B3LYP-D* optimized geometries were also performed by employing B3LYP combined with the recently proposed D3(ABC) scheme [53] for dispersion energies and the M06-D meta-GGA hybrid functional [71] which is known to provide better results for transition metal atoms [77] such as Cr and Fe.

All calculations were performed at the SuperMUC (LRZ, Germany) [78] HPC IBM iDataPlex machine powered by 16 Intel cores per node running at 2.7 GHz, with 2GB/core. On average, each calculation was run on 1000-1200 cores. An assessment of the performance of the CRYSTAL code has also been carried out to evaluate the scaling of the code on more than 1000 cores on a model system closely resembling the final model structure of MIL-100, but without any remaining symmetry. The results of the scaling and timings are reported as Supplementary Information. The scaling with the number of cores is excellent and proves the feasibility of the calculations of structure and properties performed on unit cells of thousands atoms by means of MPPCrystal on High Performance Computating facilities.

In addition, we also take advantage of the replicated data parallel version of the module Pproperties [79] of CRYSTAL to compute electron charge density and electrostatic potential 3D maps of MIL-100. Graphical representation of the 3D isosurfaces has been done with JMol [80,81].

Results and Discussion

Structure

Let us start by discussing the results about the structure of MIL-100(M^{III}) alone. The lattice parameters calculated for each isoreticular structure at the adopted level of theory and the deviation from the experimental data are reported in Table 1. The optimized structures of bulk MIL-100(M^{III}) have been reported as Crystallographic information file in the Supplementary Information.

Even though the computed structures correspond to a tetragonal space group, the difference between *a* and *c* vector is very small and the *c/a* ratio is very close to one. Therefore, a very small deviation from cubic lattice is predicted for the isoreticular family of MIL-100(M^{III}) and the optimised structures can be considered as *pseudo-cubic* with the average lattice parameter being very close to the experimental value as shown in Table 1. The percentage deviation of the unit cell volume from the experimental data is very small, it is below 1% except for Sc. In the latter case the experimental value has been measured at 298 K and the counter-ion is OH^- instead of F^-. In spite of this, the overall results are in excellent accord with experimental findings and the agreement is impressive for such a large and complex structure.

Table 1. Predicted lattice parameters (LP) of MIL-100(M^{III}) optimized at B3LYP-D*/pob-TVZP + 6-311G (d,p) level in comparison with experimental data along with the percentage deviation of volume (ΔV%). Details of the counterion used in the synthesis and structure determination of each isoreticular MIL-100 sample are also indicated [a].

M^{III}	*a*	*c*	*c/a*	*Volume*	*Mean LP*	*a*	*Volume*	*Exp. details*[a]	*ΔV%*
	Current work					Experimental data			
Al	71.531	71.494	0.9995	365816.0	71.519	71.687	368401.0	OH^-, XRSCD, 100K [43]	-0.70
Sc	74.676	74.823	1.0020	417248.2	74.725	74.350	411001.0	OH^-, XRPD, 298K [45,46]	1.52
Cr	72.602	73.249	1.0089	386097.1	72.818	72.906	387511.4	F^-, XRPD, 80K [42]	-0.36
Fe	73.158	73.302	1.0020	392311.9	73.206	73.340	394481.1	F^-, XRPD, 80K[49]	-0.55

[a] Type of counterion, experimental technique and temperature

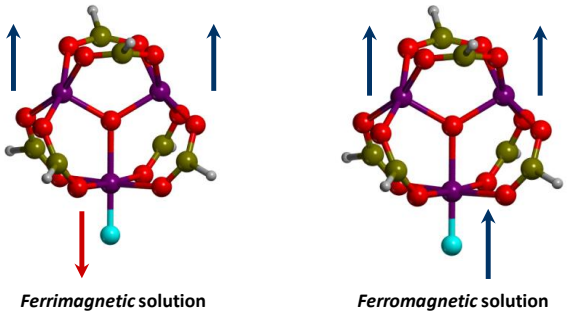

Figure 2. Schemes for the spin coupling between the unpaired electrons of the metal atoms in the inorganic secondary building unit for the two magnetic configurations of MIL-100 (Cr) and MIL-100 (Fe) investigated in the present work. Arrows represent the orientation of the total spin of the metal atom: Cr (S=3/2) and Fe (S=5/2).

For MIL-100(Cr) and MIL-100(Fe), calculations become even more complex due to the presence of unpaired electrons for the two transition metals. Two different spin state configurations have been investigated for the inorganic secondary building unit as sketched in Figure 2.

For MIL-100(Fe), in accordance with experimental evidence from Mossbauer measurements [49], we fixed the electronic configuration of iron in a high-spin state (S=5/2). Computed results show that a ferromagnetic interaction among metal atoms in the TU that tends to align the spin vectors in a parallel fashion, is disfavoured by 5.0 kJ/mol per iron atom with respect to a ferrimagnetic solution in which an antiferromagnetic interaction is present. This agrees with experiment as reported by Serre and co-workers [49]. For MIL-100(Cr) a similar ferrimagnetic solution has been found to be slightly more stable than the ferromagnetic one by 0.5 kJ/mol per Cr atom. Notably, predicted structures for MIL-100(Cr) and MIL-100(Fe) are also in very good agreement with experimental data as shown in Table 1.

The spin density 3D maps of the most stable magnetic configuration for MIL-100 with Cr and Fe isoreticular frameworks are displayed in Figure 3. As expected, unpaired electrons are mostly localized around the metal and the spin density resembles the partly occupied *d* orbitals of the atom. The spin density is also slightly spread onto the surrounding oxygens and on the counterion. This is more evident in MIL-100(Fe) than in the chromium analogue. Interestingly, while some magnetic coupling is observed within the atoms of the trimeric units, no magnetic interaction is visible between them, through the organic linkers, thus suggesting that the trimeric units act as independent moieties with respect to the magnetic ordering of the whole framework.

Electrostatic potential

Before discussing the interaction of CO_2 with the open metal sites of the MOF, it is interesting to examine the electrostatic potential generated by the framework of MIL-100(M^{III}). Indeed, the electrostatic interaction between the porous framework and gas molecules can enhance the separation of mixtures in which the components have largely different polarities. This could have large effects in the CO_2 storage capacity in MOFs. Since the quadrupole moment of CO_2 is much larger than that of H_2 molecules [82], the electrostatic interaction CO_2-MOF is already high at room temperature and low pressure.

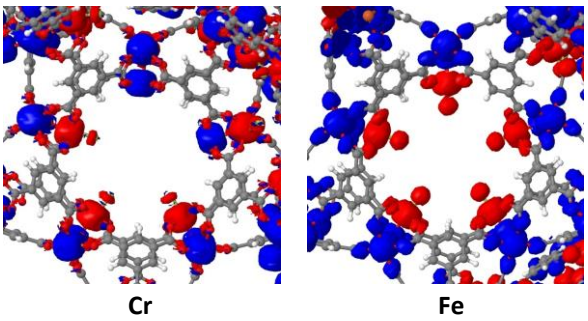

Figure 3. Spin density maps (isosurface: 0.003 e) for MIL-100(Cr) (left) and MIL-100(Fe) (right) for the ferrimagnetic electronic configuration. The spin majority is in red while the spin minority is in blue.

A useful piece of information is then provided by the electrostatic potential mapped on top of an electron charge density isosurface in that it allows us to highlight positive and negative regions showing where possible adsorption sites can be located. Figure 4 shows such a colour-coded iso-density surface

for MIL-100(Al) but very similar pictures are obtained for the isoreticular series of MIL-100 investigated in the present work. The negative regions of the electrostatic potential (in red) are dominated by the counterions. They show that the positioning of the fluorine atoms on the metal led to channels that are either fully or partially filled with the counterion. It can be also observed that oxygen atoms near the metal that carries the counterion are slightly more polarized than the ones around the open metal site. The positive regions around the open metal site are clearly visible as a blue spot. Interestingly, they are located in the pentagonal and hexagonal windows.

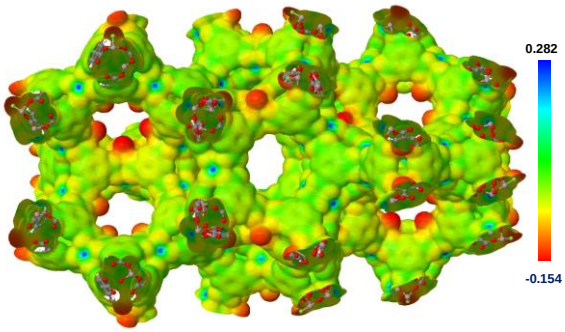

Figure 4. Electrostatic potential (in a.u.) of MIL-100(Al) as mapped on an electron charge density isosurface (0.003 e). The blue colour codifies the regions in which the potential is positive while the red colour corresponds to negative values of potential; the green colour represents the neutrality as shown in the colour scale reported on the right side of the picture.

A close inspection of the electrostatic potential of MIL-100(M^{III}) around the open metal site for the different metals, as displayed in Figure 5, highlights that Al and Cr show the most localized positive electrostatic potential, whereas for Sc it is more diffuse and the electrostatic potential is lowest on Fe.

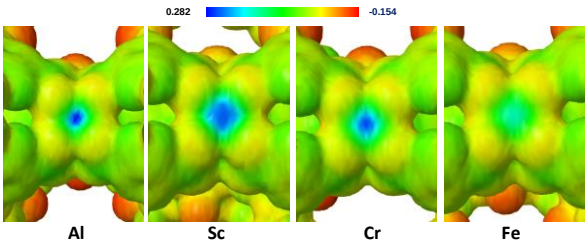

Figure 5. Electrostatic potential of MIL-100 around the open metal site with different metals, namely: Al, Sc, Cr and Fe.

Another useful and synthetic information about the electronic charge distribution is gained from a Mulliken population analysis that allows one to estimate how electrons are partitioned among the atoms or atomic orbitals. The average Mulliken atomic charges of the metals in MIL-100(M^{III}) are: +1.83 (Al); +1.54 (Sc); +1.78 (Cr); +1.04 (Fe), so Al and Cr being the most positively charged species, followed by scandium and then iron. Even if the quality of the Mulliken population analysis is disputable, the trend along the series of metals is in agreement with evidence from the electrostatic potential maps shown in Figure 5.

Adsorption of CO_2

On the basis of the optimized structures of MIL-100 (M^{III}=Al, Sc, Cr, Fe) the adsorption of CO_2 were then investigated. Nine open metal sites, non-equivalent by symmetry, are present in the framework (i.e. 136 sites in the primitive unit cell). As mentioned before, they are not exposed at the inner surface of the mesopores but they are located in the windows connecting the cages (see Figure 4). Two different adsorption sites were investigated with different coverage: a first site that corresponds to the lowest loading of adsorbed molecules in the unit cell (i.e. 8 molecules with about 6% loading) and a second site that allows adsorption of 16 molecules in the unit cell (i.e. 12% loading), hereafter they will be labelled as TU-I and TU-II, respectively (see Figure 6). For sake of simplicity and due to the cost of the calculations, the interaction of CO_2 with both sites were investigated for MIL-100 with Al and Sc while for Cr and Fe we only explored the TU-I/CO_2 complex. As shown in Figure 6, the geometry of the metal-CO_2 complex is different for the two adsorption sites. For TU-I site, the adsorbed molecule is oriented perpendicularly to the pentagonal channel and points toward the cage, while for TU-II, the carbon dioxide molecule is located in the pentagonal channel and points toward the linkers. The effect of adsorption on geometry of site and molecule can be clearly deduced by inspection of Table 2 and Table 3 which report the most relevant geometrical parameters sites before and after CO_2 complexation, respectively, for both TU-I and TU-II.

Let us discuss first the interaction of carbon dioxide with MIL-100(Al) and MIL-100(Sc) for which data are available for both adsorption sites.

In both cases, carbon dioxide interacts with the Lewis acid site through the bonding with the electron pairs on the oxygen atoms. For TU-I, an angle of 121.4 degrees is formed between Al and CO_2. The molecule is bent toward oxygen atoms closer to the counterion but still remains linear. Upon adsorption, Al-O bonds are slightly elongated, but the interaction is not strong enough to lead to a marked modification of the structure.

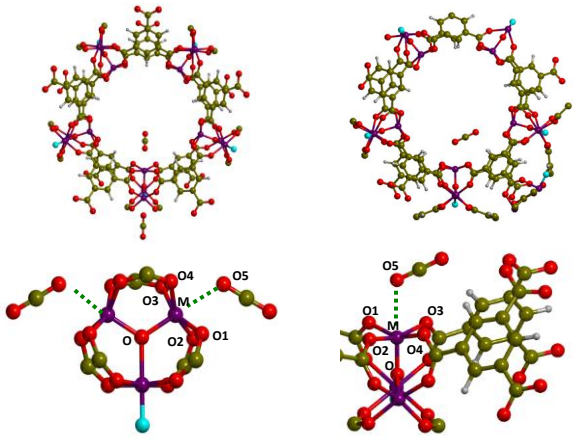

Figure 6. Investigated CO_2 adsorption sites in MIL-100 (M^{III}). On the left side, the pentagonal channel with adsorbed CO_2 on

TU-I (left side) and details of the adsorption site (right side). H, C, O, F and M, are in white, light brown, red, light blue and violet, respectively

Table 2. Relevant structural parameters describing the geometry of the TU-I and TU-II adsorption metal sites in MIL-100(M^{III}) before adsorption of CO_2 (in Å). See Figure 6 for the labelling of the atoms.

TU-I	**O-M**	**M-O1**	**M-O2**	**M-O3**	**M-O4**
Al	1.749	1.863	1.863	1.923	1.923
Sc	1.903	2.099	2.099	2.164	2.164
Cr	1.842	2.009	2.009	1.960	1.960
Fe	1.850	1.992	1.992	2.049	2.049
TU-II	**O-M**	**M-O_1**	**M-O_2**	**M-O_3**	**M-O_4**
Al	1.765	1.822	1.851	1.859	1.899
Sc	1.919	2.056	2.117	2.088	2.085

Table 3. Relevant structural parameters describing the geometry of the TU-I and TU-II adsorption metal sites in MIL-100(M^{III}) after adsorption of CO_2 (in Å and deg.). See Figure 6 for the labelling of the atoms.

TU-I/CO_2	**O-M**	**M-O1**	**M-O2**	**M-O3**	**M-O4**	**M···CO_2**	**∠M···O5-C**
Al	1.768	1.882	1.882	1.920	1.920	2.533	121.4
Sc	1.918	2.124	2.124	2.162	2.162	2.463	127.7
Cr	1.861	1.983	1.983	2.010	2.010	2.335	126.9
Fe	1.866	2.016	2.016	2.046	2.046	2.460	122.8
TU-II/CO_2	**O-M**	**M-O1**	**M-O2**	**M-O3**	**M-O4**	**M···CO_2**	**∠M···O5-C**
Al	1.775	1.820	1.861	1.870	1.890	2.780	114.5
Sc	1.937	2.052	2.105	2.108	2.111	2.515	123.7

A similar geometrical arrangement is also predicted for TU-II, but in this case the adsorbed molecule is located somewhat farther from the metal atom and is significantly bent (i.e. Al---O-C-O angle: 114.5 deg.) toward the surrounding oxygens and the linkers (see Figure 6). Even though Al shows the highest partial charge among examined metal atoms, the structure of the two adsorption sites is such that Al is buried among oxygens and is less exposed at the surface. This leads to energies of interaction weaker than expected (vide infra) from a pure electrostatic viewpoint. On the contrary, in MIL-100(Sc), Sc-O bonds are remarkably long, with the metal being more prone to interact with CO_2. Indeed, the distance between the metal and the molecule is shorter than for Al and the Sc---O-C-O angle becomes 127.7 and 123.7 deg. for TU-I and TU-II, respectively (see Table 3). Accordingly, the interaction energy is stronger as we will discuss below.

For the other MIL-100(M^{III}) structures with Cr and Fe the interaction with CO_2 on TU-I site is, not unexpectedly, more similar to Sc than Al. Cr interacts strongly with the molecule showing the shortest distance among different metal atoms. This is likely due to the high electrostatic potential and the role of partly occupied *d*-orbitals. In this respect, Fe shows a longer metal-CO_2 distance and a smaller electrostatic potential thus leading to a weaker interaction energy.

Computed interaction energies corrected for the Basis Set Superposition Error (BSSE) by means of the Counterpoise method [76] are reported in Table 4 along with the experimental values. Results show that the two adsorption sites are rather homogeneous unlike the experimental data which suggests some heterogeneity [83]. Figure 7 summarizes graphically the computed interaction energies for the CO_2 molecule interacting with the TU-I site for which full computed data are available. This permits a better comparison between metal species and highlights their different adsorption capacities. Even though the interaction energies of CO_2 decrease along the series Cr > Sc > Fe > Al, in agreement with experiments, the predicted ΔE_s appear to be definitely underestimated with respect to experimental values [84]. To better understand the role of the selected exchange-correlation functional, additional single point energy calculations on B3LYP-D* equilibrium structures have been also performed with the B3LYP-D3(ABC) method and the M06-D functional. These results are also reported in Table 4 and Figure 7. On the one hand, the inclusion of dispersion energy through the D3(ABC) model slightly increases the predicted interaction energies but it does not significantly change the trend obtained with the B3LYP-D* method. On the other hand, not unexpectedly, the M06-D gives larger interaction energies in all cases, in particular for Cr and Fe. Nevertheless, the predicted interaction energies are still underestimated with respect to the experimental adsorption

enthalpies in particular for Sc and Cr. For an even more consistent comparison with experiment, the zero-point energy and thermal correction to enthalpy should be included. On the basis of previous works [33,60], such a contribution was estimated to be about 2-4 kJ/mol. This would finally lead to a further decrease of the interaction energies, thus showing a definite underestimation by the computed data.

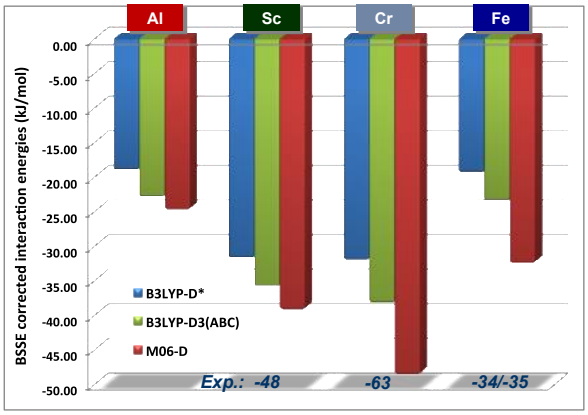

Figure 7. BSSE corrected interaction energies (in kJ/mol) for CO_2 in interaction with TU-I in MIL-100 (M^{III}=Al, Sc, Cr, Fe) (loading: 6%) as computed with B3LYP-D*, B3LYP-D3(ABC)//B3LYP-D* and M06-D//B3LYP-D*. Experimental data for adsorption enthalpy are reported for comparison.

Table 4. BSSE corrected interaction energies (in kJ/mol) for CO_2 in MIL-100(M^{III}) for TU-I and TU-II (in parenthesis) computed with the B3LYP-D*, B3LYP-D3(ABC)//B3LYP-D* and M06-D//B3LYP-D* levels. Experimental and computed data for MIL-127 are also reported for comparison.

	MIL-100				MIL-127	
M^{III}	B3LYP-D*	B3LYP-D3(ABC)[a]	M06-D[a]	Exp.	B3LYP-D*	M06-D[a]	Exp.
Al	-19.0 (-19.)	-22.9 (-23.)	-24.7		-19.3	-25.5	

Sc	-31.7 (-33.5)	-35.8 (-39.7)	-39.2	-48[84]	-32.7	-41.7
Cr	-32.0	-38.2	-48.6	-62/-63[83,84]	-29.2	-40.1
Fe	-19.4	-23.4	-32.5	-34[84] -35[50]	-21.6	-34.3
In					-32.5	-34.3	-28.5[85]

[a] Single point energy calculations on the geometry of MIL-100 optimized at the B3LYP-D*/TZVP level.

This is a puzzling and partly unexpected result because similar calculations on other MOFs have shown a rather good accuracy in the prediction of the interaction energy of small molecules with open metal sites [33,60,86]. Whether, on the one hand, this throws some doubt on the adopted computational method (i.e. B3LYP-D* and M06-D) or, on the other hand, it suggests that a deeper inspection of the experimental data is needed, now needs to be examined.

By looking at the calorimetric measurements (see Figure 3 from ref. [83]) for the adsorption of CO_2 in MIL-100(Cr) it is evident that there is a remarkably strong interaction at very low coverage, with an adsorption enthalpy of about -60 kJ/mol which rapidly decreases to lower values as soon as the coverage increases and reaches a plateau around -25 kJ/mol. This strongly indicates the presence of adsorption sites in the framework with different strength. The limit value of -25 kJ/mol is probably due to liquid-like CO_2 molecules in the pore of the structure. Indeed, this value is close to the sublimation enthalpy of carbon dioxide. Further evidence of an anomalously high adsorption enthalpy in MIL-100(Cr) is that in the same work [83] the calorimetric measurements for MIL-101(Cr) which is comprised of the same inorganic trimeric unit but different linker (i.e. 1,4-benzene-dicaboxylate) does not show the initial very strong interaction with CO_2 and the low-coverage adsorption enthalpy is in the range of 40-45 kJ/mol, closer to our computed interaction energy. Apparently, in MIL-101(Cr) the adsorption sites would seem more homogeneous than MIL-100(Cr). Nevertheless, the high adsorption enthalpy of MIL-100 with Cr and Sc has been also confirmed by spectroscopic studies [84]. Oddly, for MIL-100(Fe) experimental evidence is in better agreement with calculations. Overall, experimental data on MIL-100(Cr) appear to be not fully consistent with other isoreticular frameworks and other MOFs. Therefore, as an additional check, we decided to run similar calculations on a simpler MOF, MIL-127, that is built with the same oxo-centered inorganic unit (see Figure 1) and 3,3',5,5'-azobenzenetetracarboxylate as organic linker [87]. The unit cell of MIL-127 and the SBUs are depicted in Figure 8. As for MIL-100, MIL-127(M^{III}) possesses an isoreticular family of frameworks with different metals, where M^{III}=Al, Sc, Cr, Fe, In. Interaction energies for the different isoreticular frameworks are also reported in Table 4. In this case a single adsorption site is present in the framework. As evident, predicted results for MIL-127 are quite similar to the ones computed for MIL-100 thus indicating the accuracy of present results. Furthermore, it is worth noting that the CO_2 adsorption enthalpy for MIL-127(In) has been

determined experimentally [85]. From Table 4, it can be seen that the predicted interaction energies nicely agree with the experimental value for both B3LYP-D* and M06-D//B3LYP-D*. Interestingly, experimental data are available for an Al-based MOF with the same oxo-centered trinuclear cluster in the framework: Al-soc-MOF-1 [88]. At low loading the measured heat of adsorption is around 18 kJ/mol in good accordance with the predicted interaction energies for MIL-100 and MIL-127 with Al. This body of evidence strongly suggests that the adopted level of theory is adequate whereas the underestimated interaction energy for MIL-100(Cr) is likely due to the presence of different adsorption sites in the real system.

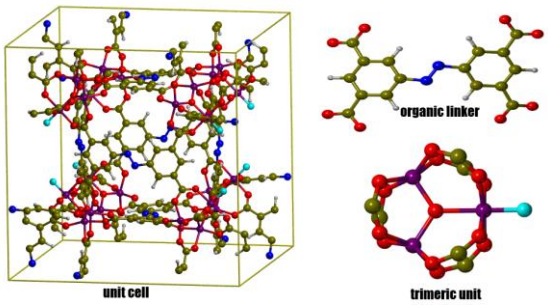

Figure 8. Crystallographic unit cell of MIL-127 and the secondary building units: the organic linker 3,3',5,5'-azobenzenetetracarboxylate and the oxo-centered trinuclear unit. H, C, O, F, N and M, are in white, light brown, red, light blue, blue and violet, respectively.

Finally, it is worth mentioning that present energetic predictions can be compared to outcomes of a recently published work [41] on cluster models of the trimeric unit adopted as a characteristic structural motif of MIL-100 and other MOFs. Clusters with increasing size were explored: a) a minimal cluster model of the trivalent metal ion (M1 in the paper); b) a cluster model of the TU with fluorine as counterion (M3XF6); c) a large cluster model in which the TU is saturated with benzoate groups (M3XB6). The results of that investigation show that predicted interaction energies and enthalpy for the large cluster model at PBE0-D3/def2-TZVPD level of calculation (i.e. -35.8 kJ/mol) is remarkably close to our findings as well as the interaction energies estimated on the smaller cluster models M1 and M3XF6 at CCSD(T) level with Cr as trivalent metal ion (i.e. -49.1 kJ/mol). The latter value is in excellent agreement with our calculated interaction energy at the M06-D//B3LYP-D* level.

Overall, the fairly good agreement between the periodic approach adopted in the present work and cluster models of ref. [41] (i) testifies that the interaction of CO_2 molecules with the open metal sites in MIL-100 is mainly localized around the adsorption site and not significantly influenced by the surrounding atoms of the framework and (ii) more importantly, supports our concern that experimental data on MIL-100(Cr) are probably not fully consistent with an ideal framework and, in turn, with a regular adsorption site as modelled in the present work.

Possible explanations for the discrepancy between computed and experimental interaction energies of MIL-100(Cr) could be (i) the presence of defective sites in the real structure of the MOF, (ii) the formation of small oxide particles within the pores, (iii) the role of the counter-ion (i.e. fluorine instead of hydroxyl groups), and (iv) the presence of water that can assist the adsorption of CO_2. As clearly demonstrated in the last years, MOFs are far from being defective free systems [89]. The role of defects in the framework is in fact an area of increasing interest in the study of MOFs. It has been recently realized that linkers can be easily missing in the structure of MOFs thus leading to either lower coordinated metal sites or different chemical environment around the adsorption site with respect to the perfect framework. Obviously, this would change the adsorption capacity of the MOF, as it would be in presence of small oxide particles. Another point that would deserve investigation is the presence of OH^- groups as counter-ions instead of fluoride. It could also happen that since water is ubiquitous, it is expected that it would easily occupy adsorption sites and may be strongly coordinated to metal sites even after thermal treatments of samples. Although all of these aspects are of interest in characterizing the adsorption properties of MIL-100, they are out of the scope of the present work and will be further explored elsewhere.

Conclusions

We have investigated the isoreticular family of the *giant* MOF MIL-100 with four different metals, namely: Al, Sc, Cr and Fe and the capture of CO_2 by open metal sites, considered as the primary adsorption sites in the framework. We have demonstrated the feasibility of periodic all-electron density functional theory calculations with hybrid functional augmented with a dispersion correction term.

In spite of the extraordinarily complex crystalline structure of MIL-100, a very satisfactory agreement with experiment is attained for the structural parameters of the empty framework. Results are even more convincing for the MOF with open shell transition metals as Cr and Fe. On the other hand, the comparison between computed interaction energies of carbon dioxide with the open metal sites of MIL-100 and experimental data is not fully satisfactory, in particular with Cr and Sc. However, we have shown that our results are consistent with a MOF with similar open metal sites and calculations on cluster models. Therefore, we believe they can be considered correct for an ideal MIL-100 framework.

Finally, even if a lot of progress has been done in the modelling of MOFs, some years ago there were still some concerns about the applicability of *ab initio* methods to large MOFs as stated by M. D. Allendorf and co-workers "...even with large parallel computers. MOFs have very large unit cells, making any computation of MOF properties highly expensive" [90]. Here, we have definitively shown that with powerful computational tools, appropriate software and high performance computing resources we can push the limit from small-to-medium frameworks to giant MOFs.

Supporting Information.

Details on the initial structure model adopted for MIL-100(Fe) and MIL-100(Cr) with the set up of the electronic configuration employed in the calculations. Scaling of MPPcrystal with the number of processors for a model system of MIL-100(M^{III}). Crystallographic data (cif format) of the B3LYP-D* optimized structures of MIL-100(M^{III}).

AUTHOR INFORMATION

Corresponding Author

* bartolomeo.civalleri@unito.it

Present Addresses

† Accenture spa, Via Maurizio Quadrio, 20154 Milano - Italy

¥ WATERVIEW srl, Via Giuseppe Pomba 23, 10123 Torino - Italy

CONFLICTS OF INTEREST

There are no conflicts of interest to declare

ACKNOWLEDGMENTS

We kindly acknowledge PRACE initiative for computing resources (Grant: Project 2013081680).

REFERENCES

(1) Long, J. R.; Yaghi, O. M. The Pervasive Chemistry of Metal–Organic Frameworks. *Chem. Soc. Rev.* **2009**, *38*, 1213-1214.

(2) Zhou, H.-C.; Long, J. R.; Yaghi, O. M. Introduction to Metal–Organic Frameworks. *Chem. Rev.* **2012**, *112*, 673–674.

(3) Tan, J.-C.; Civalleri, B. Metal–Organic Frameworks and Hybrid Materials: From Fundamentals to Applications. *CrystEngComm* **2015**, *17*, 197–198.

(4) Maurin, G.; Serre, C.; Cooper, A.; Férey, G. The New Age of MOFs and of Their Porous-Related Solids. *Chem. Soc. Rev*. **2017**, 46, 3104–3107.

(5) O'Keeffe, M.; Yaghi, O. M. Deconstructing the Crystal Structures of Metal–Organic Frameworks and Related Materials into Their Underlying Nets. *Chem. Rev.* **2012**, *112*, 675–702.

(6) Furukawa, H.; Ko, N.; Go, Y. B.; Aratani, N.; Choi, S. B.; Choi, E.; Yazaydin, A. Ö.; Snurr, R. Q.; O'Keeffe, M.; Kim, J.; et al. Ultrahigh Porosity in Metal-Organic Frameworks. *Science,* **2010**, *329*, 424–428.

(7) Moghadam, P. Z.; Li, A.; Wiggin, S. B.; Tao, A.; Maloney, A. G. P.; Wood, P. A.; Ward, S. C.; Fairen-Jimenez, D. Development of a Cambridge Structural Database Subset: A Collection of Metal-Organic Frameworks for Past, Present, and Future. *Chem. Mater*. **2017**, *29*, 2618–2625.

(8) Moghadam, P. Z.; Islamoglu, T.; Goswami, S.; Exley, J.; Fantham, M.; Kaminski, C. F.; Snurr, R. Q.; Farha, O. K.; Fairen-Jimenez, D. Computer-Aided Discovery of a Metal-Organic Framework with Superior Oxygen Uptake. *Nat. Commun.* **2018**, *9*, 1378-1385.

(9) Zhou, H. L. J. S. J. Metal–Organic Frameworks for Separation. *Adv. Mater.* **2018**, *30*, 869–932.

(10) Yang, Q.; Zhong, C.; Chen, J. F. Computational Study of CO_2 Storage in Metal-Organic Frameworks. *J. Phys. Chem. C* **2008**, *112*, 1562–1569.

(11) Sumida, K.; Rogow, D. L.; Mason, J. A.; McDonald, T. M.; Bloch, E. D.; Herm, Z. R.; Bae, T.-H.; Long, J. R. Carbon Dioxide Capture in Metal–Organic Frameworks. *Chem. Rev.* **2012**, *112*, 724–781.

(12) Yu, J.; Xie, L. H.; Li, J. R.; Ma, Y.; Seminario, J. M.; Balbuena, P. B. CO_2 Capture and Separations Using MOFs: Computational and Experimental Studies. *Chem. Rev.* **2017**, *117*, 9674-9754.

(13) Li, S.; Chung, Y. G.; Simon, C. M.; Snurr, R. Q. High-Throughput Computational Screening of Multivariate Metal-Organic Frameworks (MTV-MOFs) for CO_2 Capture. *J. Phys. Chem. Lett.* **2017**, *8*, 6135–6141.

(14) Erucar, I.; Keskin, S. High-Throughput Molecular Simulations of Metal Organic Frameworks for CO_2 Separation: Opportunities and Challenges. *Front. Mater.* **2018**, *5*.

(15) Altintas, C.; Erucar, I.; Keskin, S. High-Throughput Computational Screening of the Metal Organic Framework Database for CH_4/H_2 Separations. *ACS Appl. Mater. Interfaces* **2018**, *10*, 3668–3679.

(16) Düren, T.; Bae, Y. S.; Snurr, R. Q. Using Molecular Simulation to Characterise Metal-Organic Frameworks for Adsorption Applications. *Chem. Soc. Rev.* **2009**, *38*, 1237–1247.

(17) Fischer, M.; Gomes, J. R. B.; Jorge, M. Computational Approaches to Study Adsorption in MOFs with Unsaturated Metal Sites. *Mol. Simul.* **2014**, *40*, 537–556.

(18) Dokur, D.; Keskin, S. Effects of Force Field Selection on the Computational Ranking of MOFs for CO_2 Separations. *Ind. Eng. Chem. Res.* **2018**, *57*, 2298–2309.

(19) Montoro, C.; García, E.; Calero, S.; Pérez-Fernández, M. A.; López, A. L.; Barea, E.; Navarro, J. A. R. Functionalisation of MOF Open Metal Sites with Pendant Amines for CO_2 Capture. *J. Mater. Chem.* **2012**, *22*, 10155–10158.

(20) Dubbeldam, David; Walton, Krista S.; Vlugt, Thijs H.; Calero, S. Design, Parameterization, and Implementation of Atomic Force Fields for Adsorption in Nanoporous Materials. *Adv. Theory Simul.* **2019**. https://doi.org/doi.org/10.1002/adts.201900135.

(21) Coupry, D. E.; Addicoat, M. A.; Heine, T. Extension of the Universal Force Field for Metal-Organic Frameworks. *J. Chem. Theory Comput.* **2016**, *12*, 5215–5225.

(22) Zhao, L.; Yang, Q.; Ma, Q.; Zhong, C.; Mi, J.; Liu, D. A

Force Field for Dynamic Cu-BTC Metal-Organic Framework. *J. Mol. Model.* **2011**, *17*, 227–234.

(23) Ramsahye, N. A.; Maurin, G.; Bourrelly, S.; Llewellyn, P. L.; Devic, T.; Serre, C.; Loiseau, T.; Ferey, G. Adsorption of CO_2 in Metal Organic Frameworks of Different Metal Centres: Grand Canonical Monte Carlo Simulations Compared to Experiments. *Adsorption* **2007**, *13*, 461–467.

(24) Choomwattana, S.; Maihom, T.; Khongpracha, P.; Probst, M.; Limtrakul, J. Structures and Mechanisms of the Carbonyl-Ene Reaction between MOF-11 Encapsulated Formaldehyde and Propylene: An ONIOM Study. *J. Phys. Chem. C* **2008**, *112*, 10855–10861.

(25) Oxford, G. A. E.; Snurr, R. Q.; Broadbelt, L. J. Hybrid Quantum Mechanics/Molecular Mechanics Investigation of (Salen)Mn for Use in Metal-Organic Frameworks. *Industrial and Engineering Chemistry Research* **2010**, 49, 10965–10973.

(26) Hirao, H.; Ng, W. K. H.; Moeljadi, A. M. P.; Bureekaew, S. Multiscale Model for a Metal-Organic Framework: High-Spin Rebound Mechanism in the Reaction of the Oxoiron(IV) Species of Fe-MOF-74. *ACS Catal.* **2015**, *5*, 3287–3291.

(27) Doitomi, K.; Xu, K.; Hirao, H. The Mechanism of an Asymmetric Ring-Opening Reaction of Epoxide with Amine Catalyzed by a Metal-Organic Framework: Insights from Combined Quantum Mechanics and Molecular Mechanics Calculations. *Dalt. Trans.* **2017**, *46*, 3470–3481.

(28) Wu, X. P.; Gagliardi, L.; Truhlar, D. G. Combined Quantum Mechanical and Molecular Mechanical Method for Metal-Organic Frameworks: Proton Topologies of NU-1000. *Phys. Chem. Chem. Phys.* **2018**, *20*, 1778–1786.

(29) Wu, X. P.; Gagliardi, L.; Truhlar, D. G. Multilink F∗ Method for Combined Quantum Mechanical and Molecular Mechanical Calculations of Complex Systems. *J. Chem. Theory Comput.* **2019**, *15*, 4208–4217.

(30) Lou, J.; Xu, H.; Liu, Y.; Zhao, Y.; Daemen, L. L.; Brown, C.; Timofeeva, T. V.; Ma, S.; Zhou, H. C. Hydrogen Adsorption in a Highly Stable Porous Rare-Earth Metal-Organic Framework: Sorption Properties and Neutron Diffraction Studies. *J. Am. Chem. Soc.* **2008**, *130*, 9626–9627.

(31) Sillar, K.; Hofmann, A.; Sauer, J. Ab Initio Study of Hydrogen Adsorption in MOF-5. *J. Am. Chem. Soc.* **2009**, *131*, 4143–4150.

(32) Poloni, R.; Smit, B.; Neaton, J. B. Ligand-Assisted Enhancement of CO_2 Capture in Metal-Organic Frameworks. *J. Am. Chem. Soc.* **2012**, *134*, 6714–6719.

(33) Valenzano, L.; Civalleri, B.; Chavan, S.; Palomino, G. T.; Areán, C. O.; Bordiga, S. Computational and Experimental Studies on the Adsorption of CO, N_2, and CO_2 on Mg-MOF-74. *J. Phys. Chem. C* **2010**, *114* (25), 11185–11191. https://doi.org/10.1021/jp102574f.

(34) Poloni, R.; Smit, B.; Neaton, J. B. CO 2 Capture by Metal-Organic Frameworks with van der Waals Density Functionals. *J. Phys. Chem. A* **2012**, *116* (20), 4957–4964. https://doi.org/10.1021/jp302190v.

(35) Yang, Q.; Wiersum, A. D.; Jobic, H.; Guillerm, V.; Serre, C.; Llewellyn, P. L.; Maurin, G. Understanding the Thermodynamic and Kinetic Behavior of the CO_2/CH_4 Gas Mixture within the Porous Zirconium Terephthalate UiO-66(Zr): A Joint Experimental and Modeling Approach. *J. Phys. Chem. C* **2011**, *115*, 13768–13774.

(36) Lopez, M. G.; Canepa, P.; Thonhauser, T. NMR Study of Small Molecule Adsorption in MOF-74-Mg. *J. Chem. Phys.* **2013**, *138*, 154704.

(37) Grajciar, L.; Bludský, O.; Nachtigall, P. Water Adsorption on Coordinatively Unsaturated Sites in CuBTC MOF. *J. Phys. Chem. Lett.* **2010**, *1*, 3354–3359.

(38) Chen, L.; Morrison, C. A.; Düren, T. Improving Predictions of Gas Adsorption in Metal-Organic Frameworks with Coordinatively Unsaturated Metal Sites: Model Potentials, Ab Initio Parameterization, and Gcmc Simulations. *J. Phys. Chem. C* **2012**, *116*, 18899–18909.

(39) Lin, L. C.; Lee, K.; Gagliardi, L.; Neaton, J. B.; Smit, B. Force-Field Development from Electronic Structure Calculations with Periodic Boundary Conditions: Applications to Gaseous Adsorption and Transport in Metal-Organic Frameworks. *J. Chem. Theory Comput.* **2014**, *10*, 1477–1488.

(40) Yu, D.; Yazaydin, A. O.; Lane, J. R.; Dietzel, P. D. C.; Snurr, R. Q. A Combined Experimental and Quantum Chemical Study of CO2 Adsorption in the Metal-Organic Framework CPO-27 with Different Metals. *Chem. Sci.* **2013**, *4*, 3544–3556.

(41) Mavrandonakis, A.; Vogiatzis, K. D.; Boese, A. D.; Fink, K.; Heine, T.; Klopper, W. Ab Initio Study of the Adsorption of Small Molecules on Metal-Organic Frameworks with Oxo-Centered Trimetallic Building Units: The Role of the Undercoordinated Metal Ion. *Inorg. Chem.* **2015**, *54*, 8251–8263.

(42) Férey, G.; Serre, C.; Mellot-Draznieks, C.; Millange, F.; Surblé, S.; Dutour, J.; Margiolaki, I. A Hybrid Solid with Giant Pores Prepared by a Combination of Targeted Chemistry, Simulation, and Powder Diffraction. *Angew. Chemie - Int. Ed.* **2004**, *43*, 6296–6301.

(43) Volkringer, C.; Popov, D.; Loiseau, T.; Férey, G.; Burghammer, M.; Riekel, C.; Haouas, M.; Taulelle, F. Synthesis, Single-Crystal X-Ray Microdiffraction, and NMR Characterizations of the Giant Pore Metal-Organic Framework Aluminum Trimesate MIL-100. *Chem. Mater.* **2009**, *21*, 5695–5697.

(44) Mowat, J. P. S.; Miller, S. R.; Slawin, A. M. Z.; Seymour, V. R.; Ashbrook, S. E.; Wright, P. A. Synthesis, Characterisation and Adsorption Properties of Microporous Scandium Carboxylates with Rigid and Flexible Frameworks. *Microporous Mesoporous Mater.* **2011**, *142*, 322–333.

(45) Li, Y. T.; Cui, K. H.; Li, J.; Zhu, J. Q.; Wang, X.; Tian, Y. Q. The Giant Pore Metal-Organic Frameworks of Scandium Carboxylate with MIL-100 and MIL-101 Structures. *Chinese J. Inorg. Chem.* **2011**, *27*, 951–956.

(46) Mitchell, L.; Gonzalez-Santiago, B.; Mowat, J. P. S.; Gunn, M. E.; Williamson, P.; Acerbi, N.; Clarke, M. L.; Wright, P. A. Remarkable Lewis Acid Catalytic Performance of the Scandium Trimesate Metal Organic Framework MIL-100(Sc) for C-C and C=N Bond-Forming Reactions. *Catal. Sci. Technol.* **2013**, *3*, 606–617.

(47) Lieb, A.; Leclerc, H.; Devic, T.; Serre, C.; Margiolaki, I.; Mahjoubi, F.; Lee, J. S.; Vimont, A.; Daturi, M.; Chang, J. S. MIL-100(V) - A Mesoporous Vanadium Metal Organic Framework with Accessible Metal Sites. *Microporous Mesoporous Mater.* **2012**, *157*, 18–23.

(48) Reinsch, H.; Stock, N. Formation and Characterisation of Mn-MIL-100. *CrystEngComm* **2013**, *15*, 544–550.

(49) Horcajada, P.; Surblé, S.; Serre, C.; Hong, D. Y.; Seo, Y. K.; Chang, J. S.; Grenèche, J. M.; Margiolaki, I.; Férey, G. Synthesis and Catalytic Properties of MIL-100(Fe), an Iron(III) Carboxylate with Large Pores. *Chem. Commun.* **2007**, *100*, 2820–2822.

(50) Yoon, J. W.; Seo, Y. K.; Hwang, Y. K.; Chang, J. S.; Leclerc, H.; Wuttke, S.; Bazin, P.; Vimont, A.; Daturi, M.; Bloch, E.; et al. Controlled Reducibility of a Metal-Organic Framework with Coordinatively Unsaturated Sites for Preferential Gas Sorption. *Angew. Chemie - Int. Ed.* **2010**, *49*, 5949–5952.

(51) Grimme, S. Accurate Description of van Der Waals Complexes by Density Functional Theory Including Empirical Corrections. *J. Comput. Chem.* **2004**, *25*, 1463–1473.

(52) Grimme, S. Semiempirical GGA-Type Density Functional Constructed with a Long-Range Dispersion Correction. *J. Comput. Chem.* **2006**, *27*, 1787–1799.

(53) Grimme, S.; Antony, J.; Ehrlich, S.; Krieg, H. A Consistent and Accurate Ab Initio Parametrization of Density Functional Dispersion Correction (DFT-D) for the 94 Elements H-Pu. *J. Chem. Phys.* **2010**, *132*, 1–19.

(54) Rapacioli, M.; Spiegelman, F.; Talbi, D.; Mineva, T.; Goursot, A.; Heine, T.; Seifert, G. Correction for Dispersion and Coulombic Interactions in Molecular Clusters with Density Functional Derived Methods: Application to Polycyclic Aromatic Hydrocarbon Clusters. *J. Chem. Phys.* **2009**, *130*, 244304.

(55) Zimmerli, U.; Parrinello, M.; Koumoutsakos, P. Dispersion Corrections to Density Functionals for Water Aromatic Interactions. *J. Chem. Phys.* **2004**, *120*, 2693–2699.

(56) Civalleri, B.; Zicovich-Wilson, C. M.; Valenzano, L.; Ugliengo, P. B3LYP Augmented with an Empirical Dispersion Term (B3LYP-D*) as Applied to Molecular Crystals. *CrystEngComm* **2008**, *10*, 405–410.

(57) Ugliengo, P.; Zicovich-Wilson, C. M.; Tosoni, S.; Civalleri, B. Role of Dispersive Interactions in Layered Materials: A Periodic B3LYP and B3LYP-D* Study of Mg(OH)2, Ca(OH)2 and Kaolinite. *J. Mater. Chem.* **2009**, *19*, 2564–2572.

(58) Civalleri, B.; Maschio, L.; Ugliengo, P.; Zicovich-Wilson, C. M. Role of Dispersive Interactions in the CO Adsorption on MgO(001): Periodic B3LYP Calculations Augmented with an Empirical Dispersion Term. *Phys. Chem. Chem. Phys.* **2010**, *12*, 6382–6386.

(59) Thang, H. V.; Grajciar, L.; Nachtigall, P.; Bludský, O.; Areán, C. O.; Frýdová, E.; Bulánek, R. Adsorption of CO_2 in FAU Zeolites: Effect of Zeolite Composition. *Catal. Today* **2014**, *227*, 50–56.

(60) Valenzano, L.; Civalleri, B.; Sillar, K.; Sauer, J. Heats of Adsorption of CO and CO_2 in Metal-Organic Frameworks: Quantum Mechanical Study of CPO-27-M (M = Mg, Ni, Zn). *J. Phys. Chem. C* **2011**, *115*, 21777–21784.

(61) Shearer, G. C.; Colombo, V.; Chavan, S.; Albanese, E.; Civalleri, B.; Maspero, A.; Bordiga, S. Stability vs. Reactivity: Understanding the Adsorption Properties of Ni3(BTP)2 by Experimental and Computational Methods. *Dalt. Trans.* **2013**, *42*, 6450–6458.

(62) Grajciar, L.; Wiersum, A. D.; Llewellyn, P. L.; Chang, J. S.; Nachtigall, P. Understanding CO_2 Adsorption in CuBTC MOF: Comparing Combined DFT-Ab Initio Calculations with Microcalorimetry Experiments. *J. Phys. Chem. C* **2011**, *115*, 17925–17933.

(63) Torrisi, A.; Bell, R. G.; Mellot-Draznieks, C. Functionalized MOFs for Enhanced CO_2 Capture. *Cryst. Growth Des.* **2010**, *10*, 2839–2841.

(64) Nazarian, D.; Camp, J. S.; Chung, Y. G.; Snurr, R. Q.; Sholl, D. S. Large-Scale Refinement of Metal-Organic Framework Structures Using Density Functional Theory. *Chem. Mater.* **2017**, *29*, 2521–2528.

(65) Ramsahye, N. A.; Maurin, G.; Bourrelly, S.; Llewellyn, P. L.; Serre, C.; Loiseau, T.; Devic, T.; Férey, G. Probing the Adsorption Sites for CO_2 in Metal Organic Frameworks Materials MIL-53 (Al, Cr) and MIL-47 (V) by Density Functional Theory. *J. Phys. Chem. C* **2008**, *112*, 514–520.

(66) Vogiatzis, K. D.; Klopper, W.; Friedrich, J. Non-Covalent Interactions of CO_2 with Functional Groups of Metal-Organic Frameworks from a CCSD(T) Scheme Applicable to Large Systems. *J. Chem. Theory Comput.* **2015**, *11*, 1574–1584.

(67) Dovesi, R.; Orlando, R.; Erba, A.; Zicovich-Wilson, C. M.; Civalleri, B.; Casassa, S.; Maschio, L.; Ferrabone, M.; De La Pierre, M.; D'Arco, P.; et al. CRYSTAL14: A Program for the Ab Initio Investigation of Crystalline Solids. *Int. J. Quantum Chem.* **2014**, *114*, 1287–1317.

(68) Erba, A.; Baima, J.; Bush, I.; Orlando, R.; Dovesi, R. Large-Scale Condensed Matter DFT Simulations: Performance and Capabilities of the CRYSTAL Code. *J. Chem. Theory Comput.* **2017**, *13*, 5019–5027.

(69) Becke, A. Density-functional thermochemistry. III. The role of exact exchange. *J. Chem. Phys.* **1993**, *98*, 5648–

5652.

(70) Adamo, C.; Barone, V. Toward Reliable Density Functional Methods without Adjustable Parameters: The PBE0 Model. *J. Chem. Phys.* **1999**, *110*, 6158–6170.

(71) Zhao, Y.; Truhlar, D. G. The M06 Suite of Density Functionals for Main Group Thermochemistry, Thermochemical Kinetics, Noncovalent Interactions, Excited States, and Transition Elements: Two New Functionals and Systematic Testing of Four M06-Class Functionals and 12 Other Function. *Theor. Chem. Acc.* **2008**, *120*, 215–241.

(72) Dovesi, R.; Erba, A.; Orlando, R.; Zicovich-Wilson, C. M.; Civalleri, B.; Maschio, L.; Rérat, M.; Casassa, S.; Baima, J.; Salustro, S.; et al. Quantum-Mechanical Condensed Matter Simulations with CRYSTAL. *Wiley Interdiscip. Rev. Comput. Mol. Sci.* **2018**, *8*, e1360.

(73) Orlando, R.; Delle Piane, M.; Bush, I. J.; Ugliengo, P.; Ferrabone, M.; Dovesi, R. A New Massively Parallel Version of CRYSTAL for Large Systems on High Performance Computing Architectures. *J. Comput. Chem.* **2012**, *33*, 2276–2284.

(74) Peintinger, M. F.; Oliveira, D. V.; Bredow, T. Consistent Gaussian Basis Sets of Triple-Zeta Valence with Polarization Quality for Solid-State Calculations. *J. Comput. Chem.* **2013**, *34*, 451–459.

(75) Schäfer, A.; Horn, H.; Ahlrichs, R. Fully Optimized Contracted Gaussian Basis Sets for Atoms Li to Kr. *J. Chem. Phys.* **1992**, *97*, 2571–2577.

(76) Scroll, P.; For, D. The Calculation of Small Molecular Interactions by the Di Erences of Separate Total Energies. Some Procedures with Reduced Errors. *Mol. Phys.* **2002**, *19*, 553–566.

(77) Yu, H. S.; Li, S. L.; Truhlar, D. G. Perspective: Kohn-Sham Density Functional Theory Descending a Staircase. *J. Chem. Phys.* **2016**, *145*, 130901

(78) Leibniz Supercomputing Center, SuperMUC. https://www.lrz.de/services/compute/supermuc/systemdescription/ (accessed October 16, 2019)

(79) Casassa, S.; Erba, A.; Baima, J.; Orlando, R. Electron Density Analysis of Large (Molecular and Periodic) Systems: A Parallel Implementation. *J. Comput. Chem.* **2015**, *36*, 1940–1946.

(80) Hanson, R. M. Jmol - A Paradigm Shift in Crystallographic Visualization. *J. Appl. Crystallogr.* **2010**, *43*, 1250–1260.

(81) JMol, version 14.29.54; software for visualization. http://jmol.sourceforge.net (accessed October 16, 2019)

(82) Garberoglio, G.; Skoulidas, A. I.; Johnson, J. K. Adsorption of Gases in Metal Organic Materials: Comparison of Simulations and Experiments. *J. Phys. Chem. B* **2005**, *109*, 13094–13103.

(83) Llewellyn, P. L.; Bourrelly, S.; Serre, C.; Vimont, A.; Daturi, M.; Hamon, L.; De Weireld, G.; Chang, J. S.; Hong, D. Y.; Hwang, Y. K.; et al. High Uptakes of CO_2 and CH_4 in Mesoporous Metal-Organic Frameworks MIL-100 and MIL-101. *Langmuir* **2008**, *24*, 7245–7250.

(84) Cabello, C. P.; Rumori, P.; Palomino, G. T. Carbon Dioxide Adsorption on MIL-100(M) (M = Cr, V, Sc) Metal-Organic Frameworks: IR Spectroscopic and Thermodynamic Studies. *Microporous Mesoporous Mater.* **2014**, *190*, 234–239.

(85) Moellmer, J.; Celer, E. B.; Luebke, R.; Cairns, A. J.; Staudt, R.; Eddaoudi, M.; Thommes, M. Insights on Adsorption Characterization of Metal-Organic Frameworks: A Benchmark Study on the Novel Soc-MOF. *Microporous Mesoporous Mater.* **2010**, *129*, 345–353.

(86) Valenzano, L.; Vitillo, J. G.; Chavan, S.; Civalleri, B.; Bonino, F.; Bordiga, S.; Lamberti, C. Structure-Activity Relationships of Simple Molecules Adsorbed on CPO-27-Ni Metal-Organic Framework: In Situ Experiments vs. Theory. *Catal. Today* **2012**, *182*, 67–79.

(87) Liu, Y.; Eubank, J. F.; Cairns, A. J.; Eckert, J.; Kravtsov, V. C.; Luebke, R.; Eddaoudi, M. Assembly of Metal-Organic Frameworks (MOFs) Based on Indium-Trimer Building Blocks: A Porous MOF with Soc Topology and High Hydrogen Storage. *Angew. Chemie - Int. Ed.* **2007**, *46*, 3278–3283.

(88) Alezi, D.; Belmabkhout, Y.; Suyetin, M.; Bhatt, P. M.; Weseliński, L. J.; Solovyeva, V.; Adil, K.; Spanopoulos, I.; Trikalitis, P. N.; Emwas, A. H.; et al. MOF Crystal Chemistry Paving the Way to Gas Storage Needs: Aluminum-Based Soc -MOF for CH4, O_2, and CO_2 Storage. *J. Am. Chem. Soc.* **2015**, *137*, 13308–13318.

(89) Sholl, D. S.; Lively, R. P. Defects in Metal-Organic Frameworks: Challenge or Opportunity? *J. Phys. Chem. Lett.* **2015**, *6*, 3437–3444.

(90) Allendorf, M. D.; Schwartzberg, A.; Stavila, V.; Talin, A. A. A Roadmap to Implementing Metal-Organic Frameworks in Electronic Devices: Challenges and Critical Directions. *Chem. - A Eur. J.* **2011**, *17*, 11372–11388.

TOC GRAPHIC